Molecular Therapy
Nucleic Acids
Original Article

Exosomally derived Y RNA fragment alleviates hypertrophic cardiomyopathy in transgenic mice

Feng Huang,[1] Na Na,[1] Takeshi Ijichi,[1] Xiaokang Wu,[1] Kazutaka Miyamoto,[1] Alessandra Ciullo,[1] My Tran,[1] Liang Li,[1] Ahmed Ibrahim,[1] Eduardo Marbán,[1] and Geoffrey de Couto[1]

[1]Smidt Heart Institute, Cedars-Sinai Medical Center, 8700 Beverly Boulevard, Los Angeles, CA 90048, USA

Cardiosphere-derived cell exosomes (CDC_{exo}) and YF1, a CDC_{exo}-derived non-coding RNA, elicit therapeutic bioactivity in models of myocardial infarction and hypertensive hypertrophy. Here we tested the hypothesis that YF1, a 56-nucleotide Y RNA fragment, could alleviate cardiomyocyte hypertrophy, inflammation, and fibrosis associated with hypertrophic cardiomyopathy (HCM) in transgenic mice harboring a clinically relevant mutation in cardiac troponin I ($cTnI^{Gly146}$). By quantitative PCR, YF1 was detectable in bone marrow, spleen, liver, and heart 30 min after intravenous (i.v.) infusion. For efficacy studies, mice were randomly allocated to receive i.v. YF1 or vehicle, monitored for ambulatory and cardiac function, and sacrificed at 4 weeks. YF1 (but not vehicle) improved ambulation and reduced cardiac hypertrophy and fibrosis. In parallel, peripheral mobilization of neutrophils and proinflammatory monocytes was decreased, and fewer macrophages infiltrated the heart. RNA-sequencing of macrophages revealed that YF1 confers substantive and broad changes in gene expression, modulating pathways associated with immunological disease and inflammatory responses. Together, these data demonstrate that YF1 can reverse hypertrophic and fibrotic signaling pathways associated with HCM, while improving function, raising the prospect that YF1 may be a viable novel therapeutic candidate for HCM.

INTRODUCTION

Cardiosphere-derived cells (CDCs) have been tested clinically and preclinically in a variety of cardiovascular conditions.[1] The prevailing concept of CDC therapy posits that transplanted cells produce and secrete extracellular vesicles (e.g., exosomes; CDC_{exo}) with therapeutic payloads to target cells in a paracrine manner.[2–4] Although CDCs and CDC_{exo} are themselves promising therapeutic candidates, they suffer from a number of practical and conceptual limitations. CDCs vary in potency, require regular recourse to source tissue, and are fragile living entities that need careful storage and handling.[1] While CDC_{exo} are more durable,[1] parental CDCs are necessary for exosome production and isolation. To circumvent these limitations, we have leveraged RNA-sequencing (RNA-seq) technology to mine CDC_{exo} cargo and identify distinct molecular entities with therapeutic activity.[2,3,5] The most plentiful RNA species in CDC_{exo} is a fragment of the human Y4 gene (designated EV-YF1, or more simply YF1).[5] This exosomally abundant non-coding RNA (ncRNA) has bioactivity *in vitro* and *in vivo*:[5] macrophages exposed to YF1 increased the production of interleukin-10 (IL-10) and protected cardiomyocytes against oxidative stress. Additionally, YF1 reduced cardiomyocyte apoptosis and decreased infarct size in a rat model of myocardial infarction[5] and attenuated cardiac hypertrophy and fibrosis in mice with angiotensin II (Ang II)-induced hypertension.[6] These findings motivated us to determine whether YF1 might exert therapeutic benefits in a clinically relevant mouse model of hypertrophic cardiomyopathy (HCM).

HCM is the most common genetic illness affecting the heart and generally involves mutations of sarcomeric genes, including cardiac troponin I (cTnI).[7,8] Cardiomyocyte hypertrophy and fibrosis are the cardinal histologic abnormalities underlying the cardiac dysfunction and arrhythmias that plague HCM.[8] Here, we test the hypothesis that YF1 can reverse the pathological manifestations of hypertrophy and fibrosis in a mouse model of HCM. These mice harbor a mutation within the inhibitory domain of cTnI (R146G in mice [$cTnI^{Gly146}$]; R145G in humans), which enhances contractile function and depresses relaxation coincident with cardiomyocyte hypertrophy and fibrosis;[9] patients with this mutation exhibit severe global ventricular hypertrophy. Using an array of *in vitro* and *in vivo* assays, we show that YF1 suppresses, indeed reverses, cardiomyocyte hypertrophy and fibrosis via immunomodulation and macrophage polarization.

RESULTS

Biodistribution

To assess the biodistribution of YF1 in a mouse model of HCM, we delivered vehicle (saline) or YF1 (0.15 μg/g of body weight, as used previously in other mouse models)[5,6] acutely (via retro-orbital [r.o.] injection) to 4-month-old $cTnI^{Gly146}$ mice. Thirty min or 4 h later, we measured levels of YF1 in various tissues by quantitative PCR. Figure 1A shows that, at 30 min, YF1 was detectable above background in

Received 30 July 2020; accepted 15 April 2021;
https://doi.org/10.1016/j.omtn.2021.04.014.

Correspondence: Eduardo Marbán, Smidt Heart Institute, Cedars-Sinai Medical Center, 8700 Beverly Boulevard, Los Angeles, CA 90048, USA.
E-mail: eduardo.marban@cshs.org

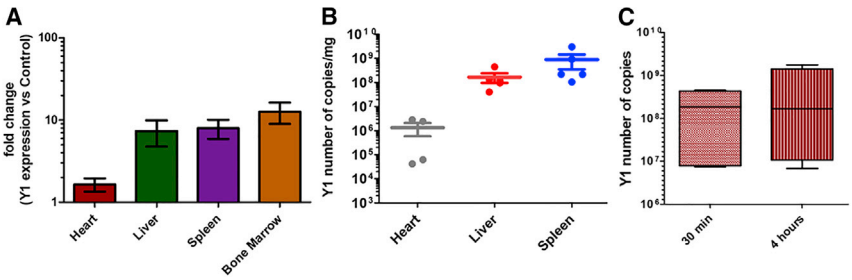

Figure 1. Biodistribution of YF1

(A) Levels of YF1 30 min post-injection expressed as fold change over background in each tissue. (B) Levels of YF1 30 min post-injection expressed as copies per mg in each of the solid organs sampled. (C) Persistent measurable levels of YF1 in heart 4 h post-injection.

all tissues sampled, with the highest levels in bone marrow, followed by spleen, liver, and heart. Normalized levels (YF1 copies per mg of tissue) showed the same rank order among the solid organs (Figure 1B). While bone marrow could not be weighed reliably before processing for RNA, its diminutive mass (estimated at <2 mg, consistent with prior quantitation[10]) relative to the solid organs (100–1,500 mg) would imply much higher levels in the marrow. Tissue levels within the heart were similar 4 h after infusion (Figure 1C), but, at that time, YF1 was not detectable in any of the other tissues. These findings indicate that YF-1 is broadly distributed within the body, with an apparent affinity for phagocytic cells such as macrophages (which are most abundant in marrow, spleen, and liver).[11]

Mobility and cardiac function in HCM mice

To assess the therapeutic efficacy of YF1 in a mouse model of HCM, we delivered vehicle (saline) or YF1 (0.15 μg/g of body weight) biweekly (via r.o. injection) to 4-month-old cTnI^{Gly146} mice over the course of 4 weeks (Figure 2A). Untreated, nontransgenic littermates (wild-type, WT) served as a control. While body weight (BW) measurements did not differ between groups (Figure 2B), YF1 significantly attenuated cardiac left ventricular (LV) wall thickness over the course of treatment (therapeutic efficacy was evident as early as 1 week following treatment, Figures 2C and 2D). At endpoint, we observed improvements in grooming behavior (qualitative observations, Figure 2E) and maximal walking capacity by treadmill (Figure 2F). Additionally, overall heart weight, but not lung weight, was normalized following YF1 treatment. Together, these data demonstrate that infusion of a single defined ncRNA, YF1, can apparently improve the well-being of cTnI^{Gly146} mice.

Cardiomyocyte hypertrophy and fibrosis are reduced with YF1 treatment

Structural remodeling of the LV in HCM is characterized by an increase in cardiomyocyte size and interstitial fibrosis.[9,12] To examine the impact of YF1 on these processes, we performed histological and molecular analyses on cardiac tissue. We observed striking decreases in interstitial LV fibrosis (Figure 3A) and cardiomyocyte hypertrophy (Figure 3B). Consistent with the histology, western blot analyses revealed significant downregulation of JNK phosphorylation, cJun expression, and Smad2 phosphorylation (Figures 3C and 3D); no significant changes were observed in P38 or P65 signaling (Figure S1). These data help rationalize the benefits of YF1, given that the JNK and Smad pathways figure prominently in hypertrophy- and fibrosis-related signaling.[13,14]

Peripheral inflammation parallels structural changes in the heart

HCM is characterized by low-grade systemic inflammation.[12,15] To assess whether YF1 modulates this response, we performed flow cytometric analyses of blood at endpoint. While no change was observed in the percentage of CD4$^+$ and CD8$^+$ lymphocytes, vehicle-treated HCM mice had reduced levels of total CD3$^+$ lymphocytes compared to WT or YF1-treated HCM mice (Figures 4A and 4B). We also noted a significant increase in Ly6C$^+$ myeloid cells in vehicle-treated HCM, which trended to decrease with YF1 treatment (Figure 4C). Decreased neutrophil (Ly6C$^+$ Ly6G$^+$) and increased monocyte (Ly6C$^+$Ly6G$^-$) populations in HCM mice receiving vehicle were normalized by YF1 treatment (Figure 4C).

YF1 suppresses inflammatory cytokines and myeloid cell mobilization to the heart

Myeloid cells mobilize to the circulation in response to chemokine gradients following injury. Thus, we analyzed serum levels of known cytokines and chemokines by protein array. Of the 40 cytokines tested (Figure S2), YF1 significantly reduced CXCL1 and TNFR1 (Figure 4D) in HCM serum, but none of the other cytokines was changed much. While TNFR1 is associated with TNF-induced inflammation and cardiovascular disease,[16] the neutrophil chemokine CXCL1 correlated with inflammatory cell mobilization (Figure 4C) and was investigated further. *Cxcl1* gene expression was significantly reduced in heart tissue from YF1-treated HCM mice (Figure 4E). To determine the source of CXCL1 expression, we cultured cardiomyocytes (neonatal rat ventricular myocytes, NRVMs) and bone marrow-derived macrophages (BMDMs) *in vitro*. In response to Ang II stimulation, NRVMs, but not BMDMs, robustly upregulated *Cxcl1* expression (Figure 4F). Next, we examined whether YF1 suppresses inflammation within the heart. Decreases in proinflammatory cytokines *Il1b* and *Il6* (Figure 5A) and monocyte marker *Cd14* (Figure 5B) were accompanied by fewer macrophages in the myocardium (Figures 5C and 5D). Together, these data demonstrate that YF1 attenuates CXCL1 expression in cardiomyocytes, reduces myeloid cell peripheral blood mobilization, suppresses proinflammatory cytokine expression, and inhibits macrophage infiltration in the heart.

Macrophages are required for YF1 activity

To test whether YF1 elicits cardioprotection via direct or indirect (immunomodulation of macrophages) effects, we stimulated NRVM

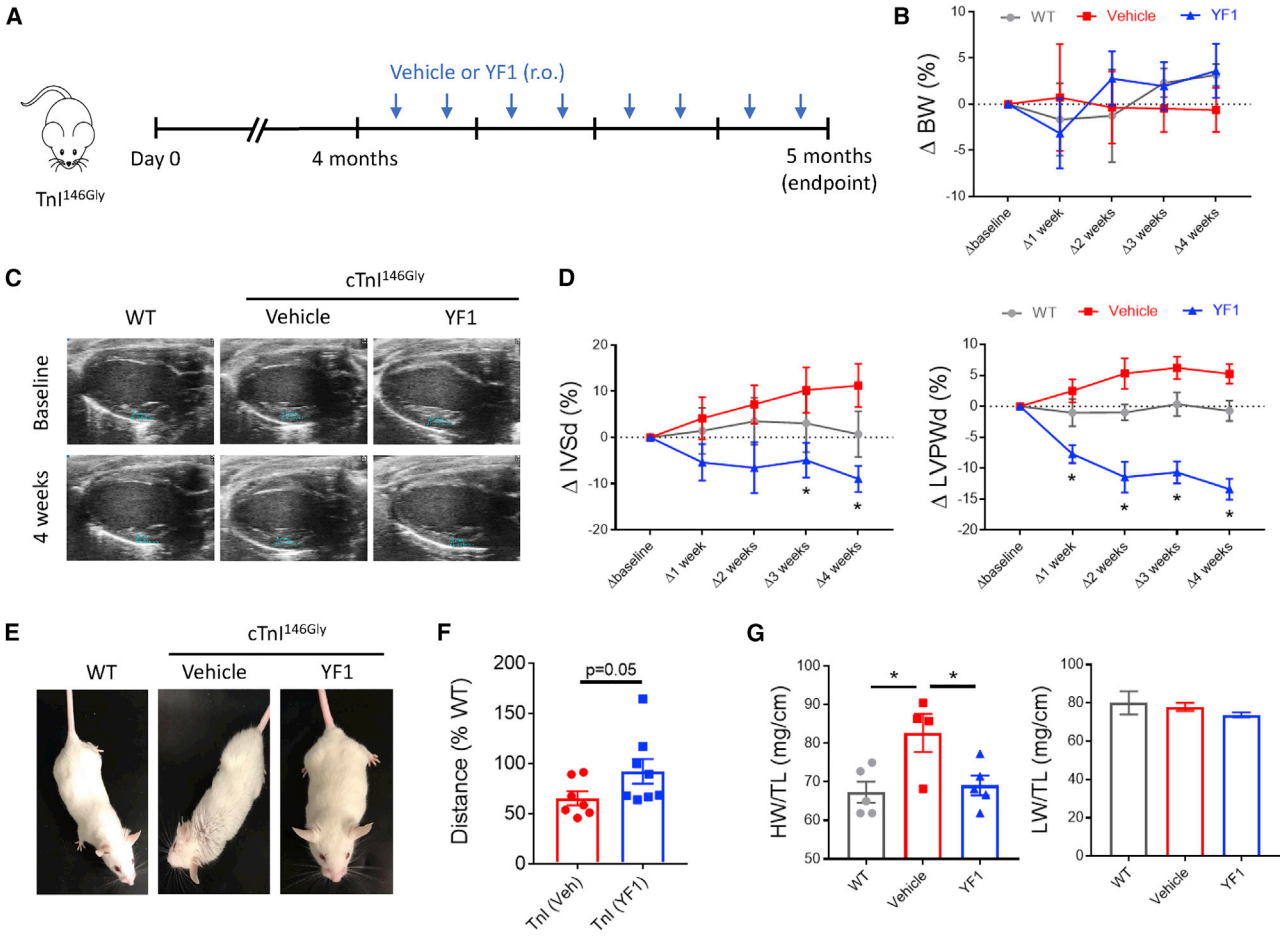

Figure 2. YF1 treatment improves mobility and cardiac function in animals with hypertrophic cardiomyopathy

(A) Schematic describing the experimental protocol for cTnI^{146Gly} mice with vehicle or YF1 treatment by retro-orbital (r.o.) injection. (B) Change in body weight (BW) over time in male and female mice. (C) Representative echocardiography images of the left ventricle in diastole. (D) Change in diastolic interventricular septal wall diameter (IVSd) and left ventricular posterior wall diameter (LVPWd) in male and female mice over time. (E) Representative images depicting grooming behavior in male and female mice in each experimental group. (F) Distance covered by treadmill in male and female mice, presented as a percentage of distance covered by WT mice. (G) Heart weight (HW)-to-tibial length (TL) ratio and lung weight (LW)-to-TL at endpoint (5 months) in male mice. Graphs depict mean ± SEM with n = 4–8/group. Statistical significance was determined using two-tailed, unpaired, Student's t test or one-way ANOVA followed by Tukey's multiple corrections test. *$p < 0.05$.

with Ang II and, 2 days later, exposed the NRVM to vehicle, YF1, or media conditioned by YF1-treated macrophages. The following day, NRVM were washed and collected for RNA extraction and gene-expression analyses (Figure 6A). YF1 had no effect on cardiomyocyte hypertrophy, while media conditioned by YF1-treated macrophages reduced the expression of *Nppa* and *Nppb* (Figure 6B). To better understand the effects of YF1 on macrophages, we exposed BMDM to vehicle or YF1 in the presence or absence of Ang II. RNA-seq revealed a dramatic shift in gene-expression profile following YF1 treatment in the presence or absence of Ang II stimulation (Figure 6C); these gene-expression changes were lost if transfection reagent was omitted when YF1 was administered (Figure S3A). The gene-expression changes were associated with several biological pathways, as determined through ingenuity pathway analysis, including pathways associated with immunological diseases and inflammatory disorders (Figures S3B and S3C). Additionally, YF1 led to increased expression of the sodium-dependent dicarboxylate transporter *Slc13a3*, independent of Ang II stimulation (Figures 6D and 6E). Slc13a3 is a high-affinity transporter, which binds a broad range of metabolic substrates (e.g., succinate and glutarate) and may skew the metabolic status of macrophages toward M1- or M2-like phenotypes.[17–19] These data reveal that YF1 alters the transcriptional landscape in unstressed and stressed macrophages and, specifically, upregulates a potent modulator of macrophage phenotype.

YF1 reverses fibrosis in aged animals with HCM

Until now, the data presented were from young adult mice (4-month-old). It seems probable that therapeutic efficacy of YF1 may wane in long-established disease. To test this idea, we implemented the same treatment protocol (2 injections per week for a period of 4 weeks) as

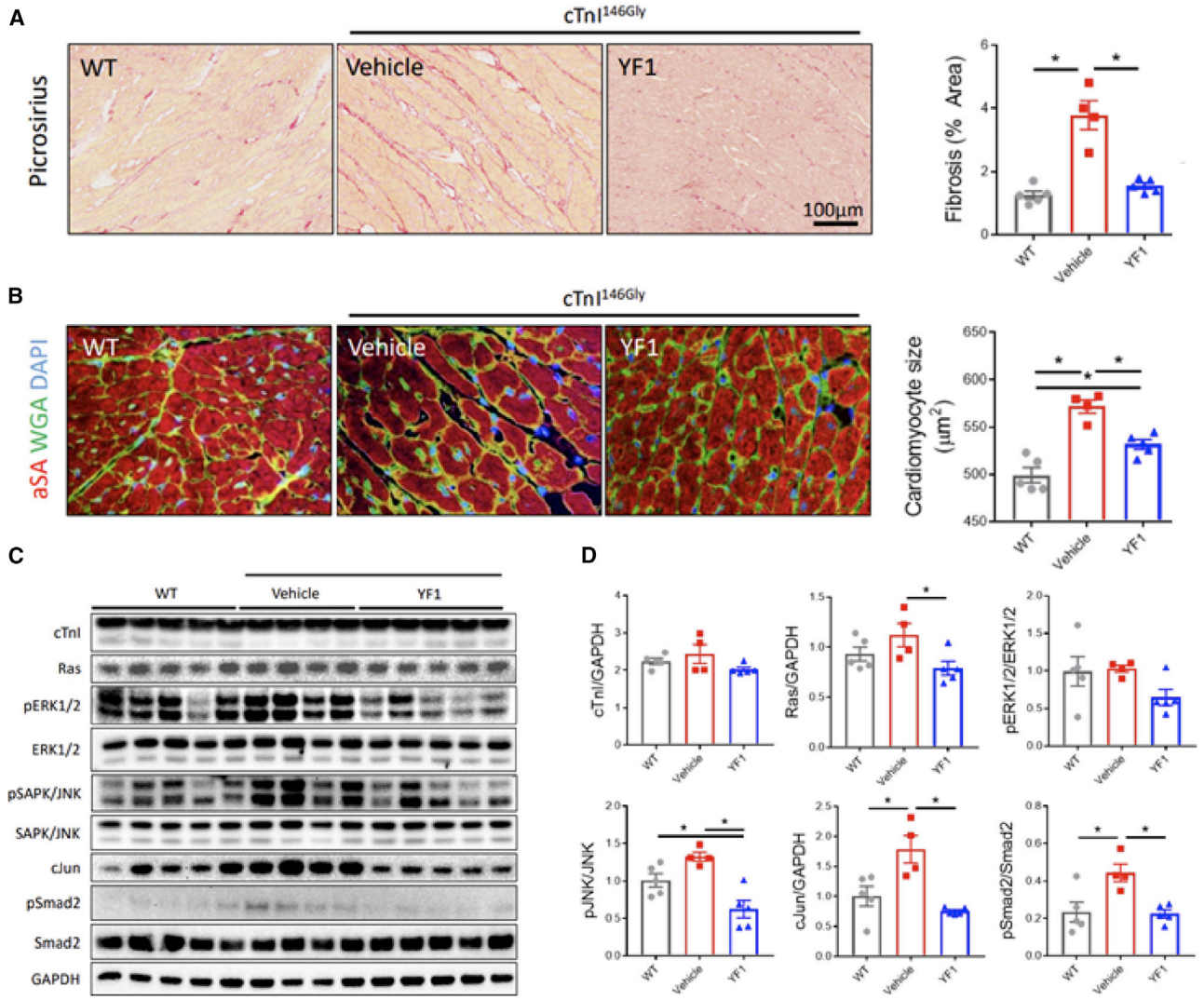

Figure 3. Cardiac fibrosis and hypertrophy are attenuated following YF1 treatment

(A) Representative images and quantification of interstitial fibrosis as determined by Picrosirius red staining. (B) Representative images and quantification of cardiomyocyte cross-sectional diameter using cell borders defined by wheat germ agglutinin (WGA), α-sarcomeric actinin (αSA), and DAPI stains. (C) Western blot images of fibrosis and hypertrophy signaling proteins. (D) Quantification of immunoblots in (C). Graphs depict mean ± SEM with n = 4–5/group. Statistical significance was determined using two-tailed, unpaired, Student's t test or one-way ANOVA followed by Tukey's multiple corrections test. *$p < 0.05$.

described earlier, but in 18-month-old cTnI^{Gly146} mice (Figure S4A). Despite a small sample size (n = 3/group), YF1 treatment trended toward an improvement in walking distance, but did not alter BW (Figure S4B). Over the course of treatment, YF1 led to a significant decrease in interventricular septum thickness at end-diastole (IVSd) and trended toward a decrease in LV posterior wall thickness at end-diastole (LVPWd) (Figure S4C). No changes in heart weight or lung weight were observed (Figure S4D). Interestingly, YF1 treatment dramatically reduced fibrosis in 2 of the 3 animals treated with YF1 (Figure S4E). While these data do not have the statistical power to conclusively demonstrate a therapeutic effect, the improvements in IVSd and fibrosis in 18-month-old cTnI^{Gly146} mice are encouraging and complement the dataset collected with 4-month-old cTnI^{Gly146} mice (Figures 2, 3, 4, 5, and 6).

DISCUSSION

HCM remains a major unmet medical need. It is the most common genetic disorder affecting the heart and accounts for a sizable fraction of morbidity and mortality in young people, particularly athletes.[20] The only widely accepted therapeutic options for HCM involve localized destruction of heart muscle (by alcohol ablation or surgical myectomy) to relieve outflow obstruction,[21] and/or the use of implantable cardioverter-defibrillators to prevent arrhythmic death.[22] Both modalities are invasive, associated with considerable risks and

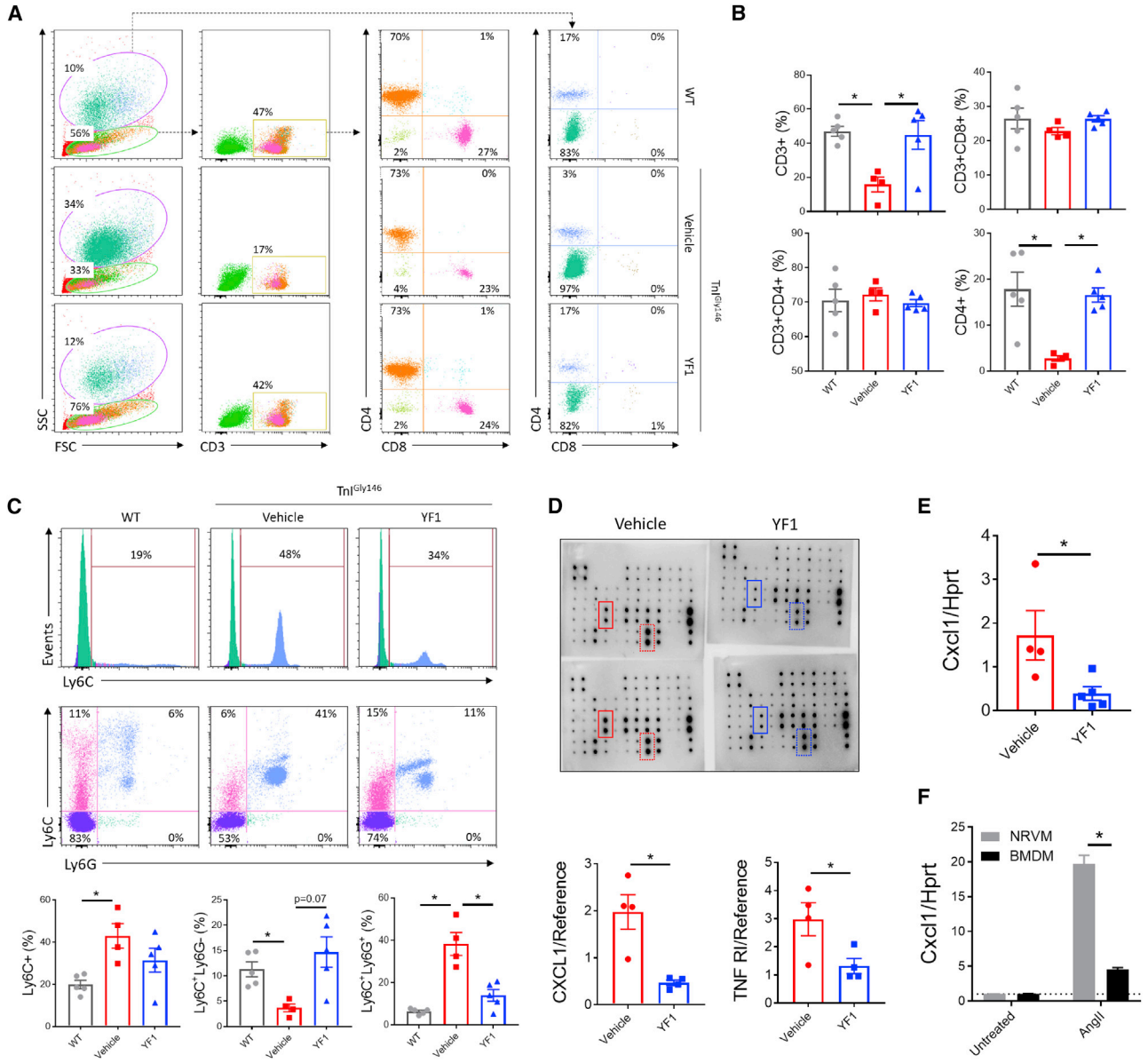

Figure 4. YF1 suppresses granulocyte and monocyte peripheral blood mobilization

(A) Representative flow plots depicting gating strategy. (B) Quantification of changes in cell populations in (A). (C) Representative flow plots and quantification of myeloid cell populations. (D) Representative image of protein array and quantification. Boxes depict proteins with significant changes in expression; CXCL1 denoted by solid border, TNF R1 denoted with dotted border. (E) Gene-expression analysis of *Cxcl1* expression in heart tissue. (F) Gene-expression analysis of *Cxcl1* in angiotensin II (AngII) treated and untreated cardiomyocytes (NRVM, neonatal rat ventricular cardiomyocytes) and macrophages (BMDM, bone marrow-derived macrophages). Graphs depict mean ± SEM with n = 4–5/group. Statistical significance was determined using two-tailed, unpaired, Student's t test or one-way ANOVA followed by Tukey's multiple corrections test. *p < 0.05.

side effects, and variably effective. Thus, new therapeutic approaches are desperately needed. A circuitous route, punctuated by serendipity, led us to test an exosomally abundant ncRNA as a therapeutic candidate in a model of HCM.

The path of discovery revealed that CDCs work by secreting exosomes that suppress or reverse fibrosis,[23,24] attenuate myocyte apoptosis,[25,26] stimulate angiogenesis,[23,27] effect immunomodulation,[2,3,28] and promote cardiomyocyte cell-cycle re-entry.[29] CDC_{exo} mediate CDC efficacy by transferring therapeutic payloads to nearby and, sometimes, distant cells.[2–4] Despite a recent claim that the effects of cell therapy are nonspecific and mimicked by infusion of dead cells or zymosan,[30] we have shown: (1) transplanted dermal fibroblasts do not mimic the effects of transplanted CDCs;[31] (2) transplanted CDCs

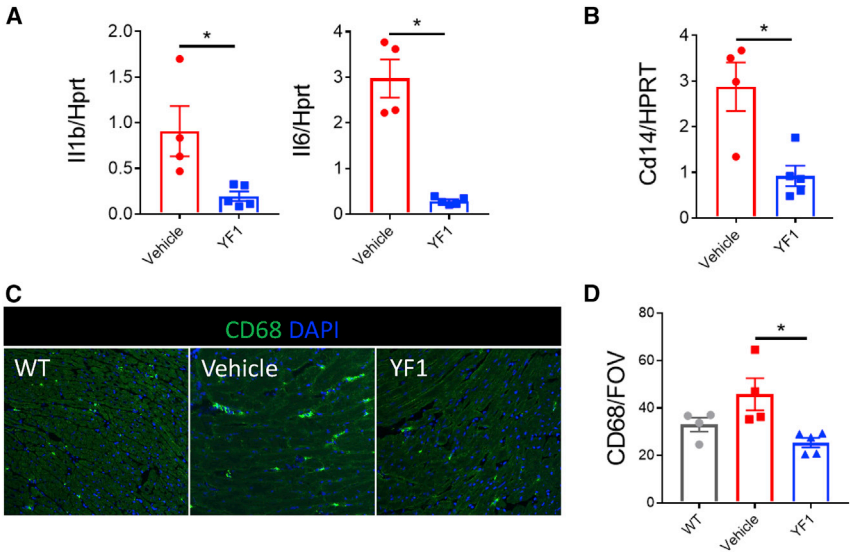

Figure 5. YF1 suppresses inflammatory cytokines and myeloid cell infiltration in the heart

(A) Gene expression of proinflammatory cytokines by qPCR. (B) Gene expression of myeloid cell marker Cd14 by qPCR. (C) Representative images of $CD68^{+}$ macrophage infiltration in the heart. (D) Quantification of immunohistochemistry in (C). Graphs depict mean ± SEM with n = 4–5/group. Statistical significance was determined using two-tailed, unpaired, Student's t test or one-way ANOVA followed by Tukey's multiple corrections test. *$p < 0.05$.

lose their bioactivity when exosome release is blocked;[2,4] and (3) CDC_{exo} mimic the benefits of CDCs in the absence of transplanted cells.[2,4] Analysis of CDC_{exo} payload using RNA-seq and proteomics revealed numerous ncRNA and proteins, some with known bioactivity and others requiring functional characterization.[2,5] To date, three distinct CDC_{exo}-derived ncRNAs have been shown to have disease-modifying bioactivity (i.e., microRNA-146a [miR-146a] in chronic ischemic cardiomyopathy,[4] miR-181b in acute MI,[2] and YF1 in renovascular hypertension).[6] YF1 is the most plentiful RNA species in CDC_{exo}, being present in >35,000 reads per sequencing run (as compared to 20–40 reads for a typical miRNA).[2,3,5] Here, we have shown YF1 bioactivity in a murine model of HCM. YF1 improves ambulatory capacity and cardiac function, decreases cardiomyocyte hypertrophy and fibrosis, suppresses inflammatory cytokines and myeloid cell mobilization to the heart, and retains disease-modifying bioactivity even in aged animals with established fibrosis and dysfunction. Moreover, the mechanism appears to reside in the immunomodulatory properties of YF1:[5,6] YF1 has no effect on isolated cardiomyocytes, and macrophages are required for YF1 activity in the HCM model. Moreover, biodistribution studies reveal intense early accumulation of YF1 in tissues (bone marrow, spleen, liver), which are particularly rich in macrophages. Thus, this exosomal Y RNA fragment antagonizes HCM via a novel pathway, providing preclinical proof-of-concept for a new treatment paradigm utilizing RNA therapeutics in HCM. The observed effects of twice-weekly intravenous YF1 encourage testing and identification of novel chemical entities and/or formulations with improved pharmacokinetics,[32] enabling less-frequent administration of pharmaceutically viable doses.

Until recently, HCM was devoid of anything but palliative treatment approaches. Mavacamten, a small molecule inhibitor of actomyosin ATPase,[33] now looks promising both in animal models and in clinical trials.[34] If, as seems likely, mavacamten advances toward registration and becomes available for clinical use, will there be a clinical need for YF1? In the absence of data, the answer remains conjectural, but it is noteworthy that the mechanisms of action differ fundamentally; mavacamten is an inhibitor of crossbridge cycling, which attenuates sarcomeric hyper-contractility, while YF1 acts via immunomodulation. Thus, it is at least theoretically possible that the two therapeutic modalities may eventually prove additive, or synergistic, in terms of therapeutic benefit.

MATERIALS AND METHODS

Animal model

All studies were performed at Cedars-Sinai Medical Center in accordance with the Institutional Animal Care and Use Committee guidelines. Female and male mice (4-month-old and 18-month-old), as detailed within the manuscript, were used for *in vivo* experimental procedures.

Transgenic $cTnI^{Gly146}$ mouse embryos (line 121) were generously donated by Jeffrey Robbins from Cincinnati Children's Hospital.[9] The Cedars-Sinai Rodent Genetics Core implanted $cTnI^{Gly146}$ embryos in female FVB surrogate mice and successfully recovered the $cTnI^{Gly146}$ transgenic mouse line. Genotype was confirmed by the Core and within our lab with specific forward (5′-GGTGGAC AAAGTGGATGAAGA-3′) and reverse (5′-TGCCACGGAGGTCA TAGA-3′) primers (Figure S1).

All mice ($cTnI^{Gly146}$ and FVB [WT, control]) were housed in a pathogen-free facility with a 14 h/10 h light/dark cycle with food and water provided *ad libitum*. Mice were maintained and bred in-house. *In vivo* experimental protocols were performed on 1- to 12-month-old female and male mice. Cardiac hypertrophy was monitored by non-invasive transthoracic echocardiography. At the designated time point, animals received vehicle (saline) or YF1 (0.15 μg/g body weight) via r.o. injection; 2 times per week over the course of 4 weeks (Figure 2A).

Echocardiography

Cardiac function and morphology were assessed by transthoracic two-dimensional and targeted M-mode echocardiography (Vevo3100, VisualSonics). Three representative cycles were captured

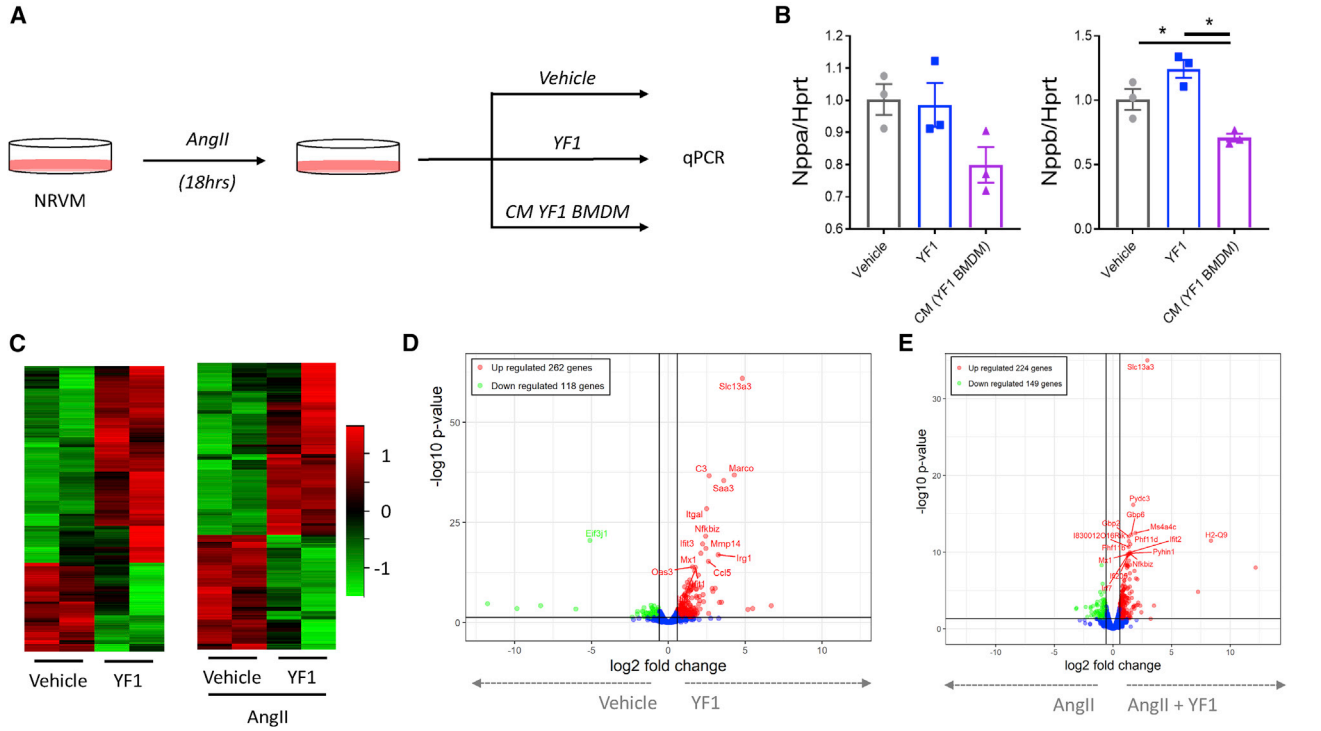

Figure 6. YF1 modifies macrophage gene profile to elicit cardioprotection

(A) Gene expression of NRVM treated with AngII studied as per the diagram of experimental workflow. (B) All groups were stimulated with AngII and then treated with vehicle (saline), YF1, or conditioned media from YF1-treated macrophages (CM YF1 BMDM). (C) Heatmap of differentially expressed genes in macrophages (left, vehicle or YF1; right, vehicle or YF1 followed by AngII treatment). (D) Volcano plot of the top differentially expressed genes in vehicle- and YF1-treated macrophages. (E) Volcano plot of the top differentially expressed genes in vehicle- and YF1-treated macrophages stimulated with AngII. Graphs depict mean ± SEM with n = 3–5/group. Statistical significance was determined using one-way ANOVA followed by Tukey's multiple corrections test. *p < 0.05.

for each animal per time point, and measurements for LV ejection fraction (LVEF), end-diastolic interventricular septal thickness (IVSd), and end-diastolic LV posterior wall thickness (LVPWd) were obtained and averaged.

Treadmill

Mice were placed inside an Exer-3/6 rodent treadmill (Columbus Instruments) at a 5-degree elevation. Animals were acclimated to the device by leaving them undisturbed for 30 min and then engaging the belt at a slow pace (10 m/min) for 20 min. After the acclimation period was complete, the exercise protocol began; shock grid activated (0.15 mA, 1Hz) and belt speed increased (1 m/min after each minute of exercise). Mice resting on the shock grid for >10 s reached maximal exercise capacity and were removed from the device.

RNA synthesis

YF1 (native and modified forms) were custom-synthesized (Integrated DNA Technologies). As reported previously,[5] the 56-nucleotide sequence for YF1 is as follows:

5′-GGCUGGUCCGAUGGUAGUGGGUUAUCAGAACUUAU UAACAUUAGUGUCACUAAAGU-3′.

Cell culture

BMDMs

Bone marrow was isolated as previously described.[35] Femurs were isolated from mouse, sterilized with 70% ethanol, flushed with PBS (containing 1% FBS and 2 mM EDTA), and filtered through a 70 μm filter. Cells were pelleted and red blood cells lysed with ACK Lysing Buffer (GIBCO). The resulting cells were resuspended in IMDM (containing 10% FBS and 10 ng/mL M-CSF [R&D Systems]) then plated and grown for 7 days to obtain macrophages.

Transfection

BMDMs were transfected with YF1 (50 nM) using Dharmafect 4 reagent (Dharmacon). After overnight incubation (∼18 h), cells were washed and collected for RNA extraction (miRNeasy Mini Kit, QIAGEN). RNA concentration and purity were determined using a NanoDrop Spectrophotometer (Thermo Scientific).

Cardiomyocytes

NRVMs were isolated and cultured as reported.[5,35] Isolated cardiomyocytes were incubated with Ang II (400 μM) in the presence of protease inhibitor (Sigma-Aldrich) to induce hypertrophy. 2 days later, vehicle, YF1, or conditioned media from YF1-treated

macrophages was added. 18 h later, cardiomyocytes were collected, and RNA isolated for gene-expression analyses.

RNA analysis

Biodistribution of EV-Y1 by qPCR

Single doses of YF1 were administered as above, and mice (n = 8) were sacrificed either 30 min (n = 4) or 4 h (n = 4) afterward. For RNA isolation, spleen, liver, and heart were excised, blotted dry, and ~20 mg sampled; bone marrow was sampled by removing both femurs, cracking them open and flushing each with ~40 mL of PBS. After RNA isolation using miRNeasy Mini Kit (QIAGEN), reverse transcription was performed using mirScript II RT Kit (QIAGEN). qPCR was done using QuantiTect SYBR Green (QIAGEN) on QuantStudio 12K Flex instrument (Applied Biosystems) with the QuantiMir universal reverse primer, EV- Y1 forward primer (5′-GGCTGGTCC GATGGTAGTG-3′), and mouse U6 forward primer (5′-TGGCC CCTGCGCAAGGATG-3′) the housekeeping gene. Fold change was calculated using $2^{(-\Delta\Delta Ct)}$, where ΔCq compares the EV-Y1 Cq value to the U6 Cq value of the same sample, and ΔΔCq compares ΔCq to that of the same organ vehicle injected. To achieve quantitation, serial dilutions of EV-Y1 were added to homogenized tissues from each organ sampled in a healthy mouse. Cq value for EV-Y1 was plotted versus the log of the number of EV-Y1 in the sample. A second order polynomial analysis was performed using GraphPad Prism 5 and the equation was used to calculate the copy number of EV-Y1 in each organ.

qPCR for transcripts

cDNA was synthesized from mRNA using High-Capacity cDNA Reverse Transcription Kit (Applied Biosystems) according to the manufacturer's protocol. The resulting cDNA was standardized across samples and mixed with TaqMan Fast Advanced Master Mix (Applied Biosystems) and pre-designed TaqMan mouse primer sets (Life Technologies, Invitrogen): *Tgfb1*, *Col1a1*, *Nppa*, *Nppb*, *Cxcl1*, *Cd14*, *Il1b*, *Il6*, and *Hprt*. Samples were amplified (QuantStudio 12K Flex Real-Time PCR system; Thermo Fisher Scientific) and analyzed by the ddCt method.

RNA-seq

The Cedars-Sinai Genomics Core performed total RNA-seq of macrophages with the Ion Total RNA-Seq Kit v2 (Life Technologies). Briefly, one microgram of total RNA was assessed for quality using a Bioanalyzer 2100 (Agilent Technologies), enriched with magnetic beads, fragmented, ligated with adapters, then reverse transcribed to make cDNA. The resulting cDNA was barcoded using Ion Xpress RNA-Seq Barcode 1-16 Kit and then amplified. RNA-seq libraries were assessed for concentration and size using the Qubit dsDNA HS Assay Kit (Life Technologies) and DNA 1000 Kit (Agilent Technologies), respectively. Samples were multiplexed and the pooled libraries were amplified onto Ion Sphere particles using an Ion PI Template OT2 200 Kit. Ion Sphere particles were then purified and prepared for sequencing (Ion Proton sequencer) using the Ion PI Sequencing 200 Kit. The raw sequencing signal was processed into FASTQ format and the adaptor was trimmed by built-in Torrent Suite software on the Proton sequencer. Alignment and reference annotation were performed as reported previously.[2]

Staining

Tissue harvest and embedding

Hearts were arrested in diastole following intra-ventricular injection of 10% potassium chloride. Hearts were excised, washed in PBS, embedded (Tissue-Tek O.C.T. Compound, Sakura), and stored at −80°C. All samples were cut (5 μm-thickness) by cryostat (Leica) and fixed (4% PFA in PBS) prior to staining.

Picrosirius red

Tissue sections were stained with Sirius Red (0.1% in Saturated Picric Acid; Electron Microscopy Sciences) according to the manufacturer's protocol. Slides were mounted (DPX; Sigma-Aldrich), and then images acquired (ScanScope AT Turbo; Aperio) and analyzed (ImageJ software). Fibrosis was determined as the percent composition per field of view.

Wheat germ agglutinin (WGA)

Tissue sections were blocked (Protein Block, Agilent Dako) and stained with α-sarcomeric actinin (αSA). Alexa Fluor 546-conjugated secondary antibody, WGA (Alexa Fluor 488-conjugated, Invitrogen), and DAPI were applied prior to mounting (Fluoroshield with DAPI, MilliporeSigma). Tissue sections were visualized by confocal microscopy (Leica) and analyzed by ImageJ software. Cardiomyocyte size was determined by measuring the area of cardiomyocytes with centrally located nuclei.

Immunohistochemistry

Tissue sections were blocked (Protein Block, Agilent Dako) and stained with primary antibody. The appropriate fluorescently conjugated secondary antibodies (Invitrogen) were applied prior to mounting (Fluoroshield with DAPI, MilliporeSigma). Tissue sections were visualized by either confocal microscopy (Leica) or cell imaging multi-mode reader (Cytation 5, Biotek) and analyzed by ImageJ software.

Immunoblotting

Protein extraction and isolation

Tissue was collected, rinsed in PBS, placed in Allprotect tissue reagent (QIAGEN), and then stored at −80°C until use. Samples were minced, suspended in T-PER Buffer (containing Halt protease and phosphatase inhibitor, Thermo Fisher), homogenized (Bead Ruptor, OMNI), and then centrifuged. Protein supernatants were collected and concentrations measured (BCA Protein Assay Kit, Pierce).

Western blot

Protein samples were prepared for gel electrophoresis (NuPAGE 4%–12% Bis-Tris, Invitrogen) according to the manufacturer's protocol. A normalized value between 10 and 30 μg was used for loading in each well. Proteins were then transferred to a Nitrocellulose Membrane, 0.45 μm (Thermo Scientific) for immunoblotting with antibodies. Bands were detected (ChemiDoc Imaging System, Bio-Rad) with ECL Western Blotting Substrate (Pierce).

Cytokine array

Serum cytokine levels were detected using a Mouse Inflammation Antibody Array (AAM-INF-1, RayBiotech) according to the manufacturer's protocol. Blood was collected and separated by centrifugation to collect serum. Membranes were blocked and incubated with serum overnight. The next day, the membranes were washed, incubated with Biotinylated Antibody Cocktail and then HRP-Streptavidin. Arrays were detected (ChemiDoc Imaging System, Bio-Rad) following the addition of detection substrate.

Flow cytometry

Peripheral blood immune cells were analyzed as reported previously.[35] Briefly, blood was collected in heparinized tubes. Red blood cells were lysed with ACK lysis buffer (GIBCO), centrifuged, and then washed with fluorescence-activated cell sorting (FACS) buffer (PBS containing 1% FBS and 2 mM EDTA). The resulting white blood cell suspension was stained with the fluorescently conjugated antibodies, washed, and analyzed (SA3800 Spectral Analyzer, Sony) based on their marker profile.

SUPPLEMENTAL INFORMATION

Supplemental information can be found online at https://doi.org/10.1016/j.omtn.2021.04.014.

ACKNOWLEDGMENTS

We thank Jeff Robbins (Cincinnati Children's Hospital) for generously providing frozen embryos for the transgenic mice. The work was supported by NIH (R01 HL124074 to E.M.), with additional general support from R01 HL142579 to G.d.C. and R01 HL133835 to E.M.

AUTHOR CONTRIBUTIONS

F.H., N.N., T.I., X.W., M.T., L.L., K.M., and A.C. performed experiments. G.d.C. and E.M. conceived the project and designed the experiments. F.H., N.N., T.I., X.W., M.T., L.L., A.I., K.M., and G.d.C. performed data analyses. G.d.C. and E.M. wrote the manuscript.

DECLARATION OF INTERESTS

E.M. owns founder's equity in Capricor, Inc. G.d.C. was a paid part-time consultant for Capricor, Inc. The other authors declare no competing interests.

REFERENCES

1. Marbán, E. (2018). A mechanistic roadmap for the clinical application of cardiac cell therapies. Nat. Biomed. Eng. *2*, 353–361.
2. de Couto, G., Gallet, R., Cambier, L., Jaghatspanyan, E., Makkar, N., Dawkins, J.F., Berman, B.P., and Marbán, E. (2017). Exosomal microRNA transfer into macrophages mediates cellular postconditioning. Circulation *136*, 200–214.
3. de Couto, G., Jaghatspanyan, E., DeBerge, M., Liu, W., Luther, K., Wang, Y., Tang, J., Thorp, E.B., and Marbán, E. (2019). Mechanism of enhanced MerTK-dependent macrophage efferocytosis by extracellular vesicles. Arterioscler. Thromb. Vasc. Biol. *39*, 2082–2096.
4. Ibrahim, A.G., Cheng, K., and Marbán, E. (2014). Exosomes as critical agents of cardiac regeneration triggered by cell therapy. Stem Cell Reports *2*, 606–619.
5. Cambier, L., de Couto, G., Ibrahim, A., Echavez, A.K., Valle, J., Liu, W., Kreke, M., Smith, R.R., Marbán, L., and Marbán, E. (2017). Y RNA fragment in extracellular vesicles confers cardioprotection via modulation of IL-10 expression and secretion. EMBO Mol. Med. *9*, 337–352.
6. Cambier, L., Giani, J.F., Liu, W., Ijichi, T., Echavez, A.K., Valle, J., and Marbán, E. (2018). Angiotensin II-induced end-organ damage in mice is attenuated by human exosomes and by an exosomal Y RNA fragment. Hypertension *72*, 370–380.
7. Kimura, A., Harada, H., Park, J.E., Nishi, H., Satoh, M., Takahashi, M., Hiroi, S., Sasaoka, T., Ohbuchi, N., Nakamura, T., et al. (1997). Mutations in the cardiac troponin I gene associated with hypertrophic cardiomyopathy. Nat. Genet. *16*, 379–382.
8. Marian, A.J., and Braunwald, E. (2017). Hypertrophic Cardiomyopathy: Genetics, Pathogenesis, Clinical Manifestations, Diagnosis, and Therapy. Circ. Res. *121*, 749–770.
9. James, J., Zhang, Y., Osinska, H., Sanbe, A., Klevitsky, R., Hewett, T.E., and Robbins, J. (2000). Transgenic modeling of a cardiac troponin I mutation linked to familial hypertrophic cardiomyopathy. Circ. Res. *87*, 805–811.
10. Nombela-Arrieta, C., and Manz, M.G. (2017). Quantification and three-dimensional microanatomical organization of the bone marrow. Blood Adv. *1*, 407–416.
11. Paoletti, R., Notario, A., and Ricevuti, G. (1997). Phagocytes: biology, physiology, pathology, and pharmacotherapeutics (New York Academy of Sciences).
12. Fang, L., Ellims, A.H., Beale, A.L., Taylor, A.J., Murphy, A., and Dart, A.M. (2017). Systemic inflammation is associated with myocardial fibrosis, diastolic dysfunction, and cardiac hypertrophy in patients with hypertrophic cardiomyopathy. Am. J. Transl. Res. *9*, 5063–5073.
13. Choukroun, G., Hajjar, R., Fry, S., del Monte, F., Haq, S., Guerrero, J.L., Picard, M., Rosenzweig, A., and Force, T. (1999). Regulation of cardiac hypertrophy in vivo by the stress-activated protein kinases/c-Jun NH(2)-terminal kinases. J. Clin. Invest. *104*, 391–398.
14. Khalil, H., Kanisicak, O., Prasad, V., Correll, R.N., Fu, X., Schips, T., Vagnozzi, R.J., Liu, R., Huynh, T., Lee, S.J., et al. (2017). Fibroblast-specific TGF-β-Smad2/3 signaling underlies cardiac fibrosis. J. Clin. Invest. *127*, 3770–3783.
15. Kuusisto, J., Kärjä, V., Sipola, P., Kholová, I., Peuhkurinen, K., Jääskeläinen, P., Naukkarinen, A., Ylä-Herttuala, S., Punnonen, K., and Laakso, M. (2012). Low-grade inflammation and the phenotypic expression of myocardial fibrosis in hypertrophic cardiomyopathy. Heart *98*, 1007–1013.
16. Carlsson, A.C., Östgren, C.J., Nystrom, F.H., Länne, T., Jennersjö, P., Larsson, A., and Ärnlöv, J. (2016). Association of soluble tumor necrosis factor receptors 1 and 2 with nephropathy, cardiovascular events, and total mortality in type 2 diabetes. Cardiovasc. Diabetol. *15*, 40.
17. Pajor, A.M. (2014). Sodium-coupled dicarboxylate and citrate transporters from the SLC13 family. Pflugers Arch. *466*, 119–130.
18. Mills, E.L., Kelly, B., Logan, A., Costa, A.S.H., Varma, M., Bryant, C.E., Tourlomousis, P., Däbritz, J.H.M., Gottlieb, E., Latorre, I., et al. (2016). Succinate Dehydrogenase Supports Metabolic Repurposing of Mitochondria to Drive Inflammatory Macrophages. Cell *167*, 457–470.e13.
19. Palmieri, E.M., Menga, A., Martín-Pérez, R., Quinto, A., Riera-Domingo, C., De Tullio, G., Hooper, D.C., Lamers, W.H., Ghesquière, B., McVicar, D.W., et al. (2017). Pharmacologic or Genetic Targeting of Glutamine Synthetase Skews Macrophages toward an M1-like Phenotype and Inhibits Tumor Metastasis. Cell Rep. *20*, 1654–1666.
20. Yotti, R., Seidman, C.E., and Seidman, J.G. (2019). Advances in the Genetic Basis and Pathogenesis of Sarcomere Cardiomyopathies. Annu. Rev. Genomics Hum. Genet. *20*, 129–153.
21. Douglas, J.S., Jr. (2020). Current state of the roles of alcohol septal ablation and surgical myectomy in the treatment of hypertrophic obstructive cardiomyopathy. Cardiovasc. Diagn. Ther. *10*, 36–44.
22. Goff, Z.D., and Calkins, H. (2019). Sudden death related cardiomyopathies - Hypertrophic cardiomyopathy. Prog. Cardiovasc. Dis. *62*, 212–216.
23. Tseliou, E., de Couto, G., Terrovitis, J., Sun, B., Weixin, L., Marbán, L., and Marbán, E. (2014). Angiogenesis, cardiomyocyte proliferation and anti-fibrotic effects underlie

structural preservation post-infarction by intramyocardially-injected cardiospheres. PLoS ONE *9*, e88590.

24. Tseliou, E., Fouad, J., Reich, H., Slipczuk, L., de Couto, G., Aminzadeh, M., Middleton, R., Valle, J., Weixin, L., and Marbán, E. (2015). Fibroblasts Rendered Antifibrotic, Antiapoptotic, and Angiogenic by Priming With Cardiosphere-Derived Extracellular Membrane Vesicles. J. Am. Coll. Cardiol. *66*, 599–611.

25. Cheng, K., Malliaras, K., Li, T.S., Sun, B., Houde, C., Galang, G., Smith, J., Matsushita, N., and Marbán, E. (2012). Magnetic enhancement of cell retention, engraftment, and functional benefit after intracoronary delivery of cardiac-derived stem cells in a rat model of ischemia/reperfusion. Cell Transplant. *21*, 1121–1135.

26. Li, T.S., Cheng, K., Malliaras, K., Matsushita, N., Sun, B., Marbán, L., Zhang, Y., and Marbán, E. (2011). Expansion of human cardiac stem cells in physiological oxygen improves cell production efficiency and potency for myocardial repair. Cardiovasc. Res. *89*, 157–165.

27. Chimenti, I., Smith, R.R., Li, T.S., Gerstenblith, G., Messina, E., Giacomello, A., and Marbán, E. (2010). Relative roles of direct regeneration versus paracrine effects of human cardiosphere-derived cells transplanted into infarcted mice. Circ. Res. *106*, 971–980.

28. de Couto, G. (2019). Macrophages in cardiac repair: Environmental cues and therapeutic strategies. Exp. Mol. Med. *51*, 1–10.

29. Malliaras, K., Zhang, Y., Seinfeld, J., Galang, G., Tseliou, E., Cheng, K., Sun, B., Aminzadeh, M., and Marbán, E. (2013). Cardiomyocyte proliferation and progenitor cell recruitment underlie therapeutic regeneration after myocardial infarction in the adult mouse heart. EMBO Mol. Med. *5*, 191–209.

30. Vagnozzi, R.J., Maillet, M., Sargent, M.A., Khalil, H., Johansen, A.K.Z., Schwanekamp, J.A., York, A.J., Huang, V., Nahrendorf, M., Sadayappan, S., and Molkentin, J.D. (2020). An acute immune response underlies the benefit of cardiac stem cell therapy. Nature *577*, 405–409.

31. Smith, R.R., Barile, L., Cho, H.C., Leppo, M.K., Hare, J.M., Messina, E., Giacomello, A., Abraham, M.R., and Marbán, E. (2007). Regenerative potential of cardiosphere-derived cells expanded from percutaneous endomyocardial biopsy specimens. Circulation *115*, 896–908.

32. Grijalvo, S., Alagia, A., Jorge, A.F., and Eritja, R. (2018). Covalent Strategies for Targeting Messenger and Non-Coding RNAs: An Updated Review on siRNA, miRNA and antimiR Conjugates. Genes (Basel) *9*, 74.

33. Green, E.M., Wakimoto, H., Anderson, R.L., Evanchik, M.J., Gorham, J.M., Harrison, B.C., Henze, M., Kawas, R., Oslob, J.D., Rodriguez, H.M., et al. (2016). A small-molecule inhibitor of sarcomere contractility suppresses hypertrophic cardiomyopathy in mice. Science *351*, 617–621.

34. Ho, C.Y., Olivotto, I., Jacoby, D., Lester, S.J., Roe, M., Wang, A., Waldman, C.B., Zhang, D., Sehnert, A.J., and Heitner, S.B. (2020). Study Design and Rationale of EXPLORER-HCM: Evaluation of Mavacamten in Adults With Symptomatic Obstructive Hypertrophic Cardiomyopathy. Circ Heart Fail *13*, e006853.

35. de Couto, G., Liu, W., Tseliou, E., Sun, B., Makkar, N., Kanazawa, H., Arditi, M., and Marbán, E. (2015). Macrophages mediate cardioprotective cellular postconditioning in acute myocardial infarction. J. Clin. Invest. *125*, 3147–3162.